

TRANSIENT FIELD MEASUREMENTS OF g -FACTORS FOR ^{24}Mg AND ^{26}Mg

J. L. EBERHARDT, R. E. HORSTMAN, H. W. HEEMAN and G. VAN MIDDELKOOP
Fysisch Laboratorium, Rijksuniversiteit, Utrecht, The Netherlands

Received 14 May 1974

Abstract: The g -factors of the first-excited $J^\pi = 2^+$ states of ^{24}Mg and ^{26}Mg have been measured with the ion-implantation perturbed angular correlation technique (IMPAC). The precession of the spins of nuclei recoiling into a magnetized iron backing is predominantly caused by the transient magnetic field for these very light and short-lived ($\tau_m \approx 1$ ps) nuclei. The transient field, which attains a value of 200 T for the Mg isotopes, is present only during the slowing-down of the recoiling nucleus and results in average precession angles of about 1.5 mrad. The experimental results are treated in the framework of the transient field theory of Lindhard and Winther. This yields g -factors of $g = +0.42 \pm 0.09$ and $g = +1.3 \pm 0.3$ for ^{24}Mg and ^{26}Mg , respectively. The results are compared with theoretical predictions and for ^{24}Mg also with a recent time-differential deorientation experiment.

E

NUCLEAR REACTION $^{24}\text{Mg}(\alpha, \alpha'\gamma)$, $E = 7.24$ MeV; $^{26}\text{Mg}(\alpha, \alpha'\gamma)$, $E = 7.89$ MeV; measured $\alpha'\gamma(\theta, B)$ in polarized Fe. $^{24,26}\text{Mg}$ deduced g for first 2^+ states. Enriched targets. IMPAC.

1. Introduction

The measurement of nuclear magnetic dipole moments can provide a sensitive test of nuclear models, since the magnetic moment is described by the wave function of one state only. For the sd shell, extensive shell-model calculations have been performed¹⁾, but few magnetic dipole moments of excited states have been measured^{2–6)}†, due to the very short lifetimes of most states in this mass region.

The present paper reports the use of the ion-implantation perturbed angular correlation technique (IMPAC)⁷⁾ to measure the g -factors of the first excited states of ^{24}Mg and ^{26}Mg recoiling in polarized iron. For such short-lived states ($\tau_m \approx 1$ ps) the measured precession of the angular correlation is attributed mainly to a transient magnetic field experienced by the ion slowing down in a polarized ferromagnetic medium. The properties of the transient field were first investigated by Borchers *et al.*^{8–10)} and were subsequently treated theoretically by Lindhard and Winther¹¹⁾. In their paper Lindhard and Winther postulate that as the electrons in the medium are scattered by the attractive Coulomb potential of the moving ion, their density is strongly enhanced. Thus the polarized electrons in a ferromagnet give rise to a strong magnetic field at the nucleus of the moving ion. The theory well reproduces the measured trends of the dependence of the transient field on the velocity^{12–14)} and

† Four recent measurements are reported in ref. 47).

atomic number of the recoiling ion in Fe and Gd, but the predicted magnitudes are about a factor of two too small¹¹⁾).

Previous transient field measurements have been performed for nuclei with atomic number $Z \geq 26$ and for states with mean lives in the range 1.4–80 ps. In the present work the method has been extended to much lighter nuclei in the sd shell, for which, although the expected precession angles are small (a few mrad), due to the short lifetimes the precession is caused almost entirely by the transient field. Corrections necessitated by the static hyperfine field are small. The main uncertainty in the interpretation of the results stems from the imperfect knowledge of the transient field¹¹⁾. It will be shown in subsect. 3.2, that all presently available transient field data can be used to fit one effective parameter in the theory, the polarized electron velocity v_p .

After the present measurements were completed the g -factor of the $J^\pi = 2^+$ state of ^{24}Mg was measured in this laboratory with the time-differential deorientation technique³⁾. The result is in excellent agreement with that reported here.

2. Experimental procedure

2.1. EXPERIMENTAL SET-UP

The 1.37 MeV level of ^{24}Mg and the 1.81 MeV level of ^{26}Mg were excited by inelastic α -particle scattering. Beams of He^+ ions from the Utrecht 6 MV tandem accelerator were focussed onto the target through a 1 mm diam. diaphragm. Bombarding energies of 7.24 and 7.89 MeV were used for ^{24}Mg and ^{26}Mg , respectively, giving optimal yield for the first excited states and leading to recoil energies of 3.14 and 3.15 MeV, respectively.

Targets were prepared from isotopically pure ^{24}Mg and ^{26}Mg , enriched respectively to 99.94 % and 99.42 %[†], by vacuum evaporation onto 10 mg/cm² thick pure Fe and 0.5 mm thick Cu backings. The targets of ^{24}Mg on Fe and Cu had thicknesses of 120 and 150 $\mu\text{g}/\text{cm}^2$, respectively, and for the ^{26}Mg targets these thicknesses were 200 and 400 $\mu\text{g}/\text{cm}^2$.

The targets were positioned in an external magnetic field of 0.15 T, the direction of which was regularly reversed (see subsect. 2.3).

Inelastically scattered α -particles were detected in a 200 μm thick annular surface-barrier Si-detector, which subtended angles between 168° and 175°. Gamma rays were detected in four 12.7 cm \times 12.7 cm NaI(Tl) crystals at angles $\pm 72^\circ$ and $\pm 108^\circ$ with respect to the beam direction and at 20 cm distance from the target. A 125 cm³ Ge(Li) detector with an efficiency of 25 % at 1.33 MeV was placed at an angle of 20° to check that the target remained in good contact with the backing throughout the measurement. No loss of contact was observed. The Doppler-shift line-shapes in the Ge(Li) detector were used to check the mean lives of the ^{24}Mg and ^{26}Mg first excited states. The agreement with the values from ref. 2) is good.

[†] Oak Ridge National Laboratory specifications.

Coincident α - γ events were recorded by an on-line CDC 1700 computer system and stored on magnetic tape.

2.2. PREPARATION OF THE Fe BACKING

The iron foils[†] were annealed for half an hour in a 200 torr H_2 atmosphere at about 700 °C. This process also reduces the oxide layers on the foils. The Mg material was evaporated onto the foils without exposing the foils further to air. The magnetization as a function of the external magnetic induction was obtained by measuring the force exerted on an accurately weighed sample in a magnetic field gradient. The magnetization corresponds to the average number of polarized electrons, ζ , per Fe atom. The result is displayed in fig. 1. It is clear that for a magnetic induction of $B > 0.07$ T the iron is saturated, with an average value $\zeta = 2.02 \pm 0.08$ from a fit to the data. This is 10 % lower than the full saturation value of $\zeta = 2.2$ expected in Fe.

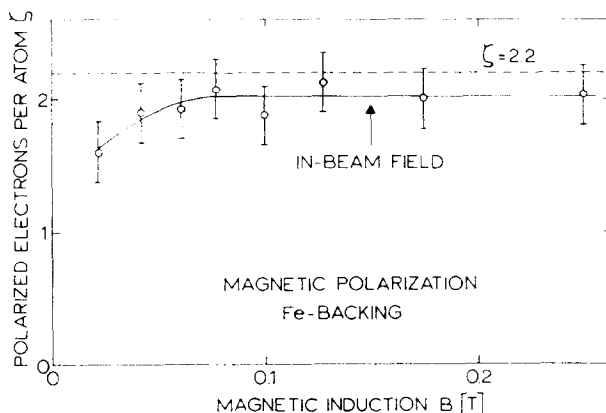


Fig. 1. Measured magnetization of a 10 mg/cm² Fe foil as a function of the applied magnetic induction B . The arrow indicates the field used in the experiments.

2.3. EXPERIMENTAL CONDITIONS

In preliminary runs the precession effect was found to decrease after about 18 h with a beam of 50 nA, probably due to radiation damage caused by the implantation of Mg and α -particles into the Fe backing. Hence, during both experiments a new area of the target was exposed to the beam every 6 h. No systematic decrease of the effect was found within this time with beam currents of 100 nA for ^{24}Mg and 60 nA for ^{26}Mg .

Measurements of the effect in Fe and of beam bending (see subject. 2.4) in Cu were alternated to minimize possible systematic effects. For ^{24}Mg a total of 5 d was spent measuring the effect and 2 d measuring beam bending, and for ^{26}Mg these periods were 6 and 4 d, respectively.

[†] Manufactured by Ventron Corp. Massachusetts, U.S.A.

The magnetic field was automatically reversed approximately every 5 min, after a preset amount of charge had been collected on the target. To ensure a reproducible magnetization of the Fe backing, a larger current than that required to maintain the induction of $B = 0.15$ T was applied to the magnet coils for the first few seconds after reversing. A label bit was set at the computer to indicate the field direction. During reversal of direction the beam was interrupted.

2.4. BEAM BENDING

A small electromagnet was used to polarize the Fe backings. Special care was taken to minimize the fringing field between the target and the α -particle detector. Such a field bends both the incoming and the outgoing α -particle trajectories. This beam bending effect slightly turns the recoil direction and this results in a rotation of the γ -ray correlation indistinguishable from that due to precession. The position of the beam spot also shifts slightly, but as this is of the order of $1\text{ }\mu\text{m}$, the influence on the γ -ray counting rates is negligible.

The magnet set-up with the target and detector chambers is shown in fig. 2. The shape of the pole faces reduces the fringing field on the detector side. This was further improved by a pure Fe shield from the target up to and including the Si detector. The target chamber downstream from the target was made of 0.5 mm thick brass. In the absence of a target, the beam can be focussed into a small tantalum cup. The orientation of the γ -ray detectors is shown in horizontal cross section in the figure.

The magnetic induction measured along the beam axis is given in fig. 3. The position $D = 0$ corresponds to the end of the Fe snout. The target is positioned at $D = 1.5$ mm, where a magnetic induction of $B = 0.15$ T is maintained. The value of $\int B ds$ over the target-detector trajectory is 3.7×10^{-4} Tm. From this a beam

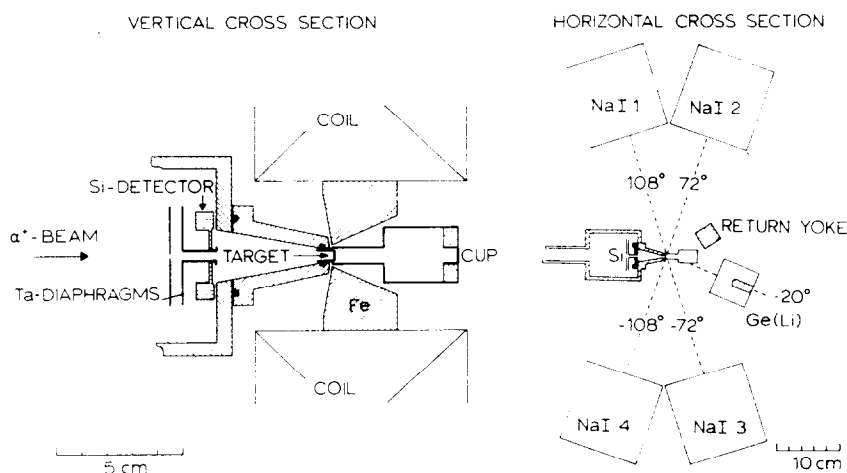


Fig. 2. Schematic of the experimental set-up.

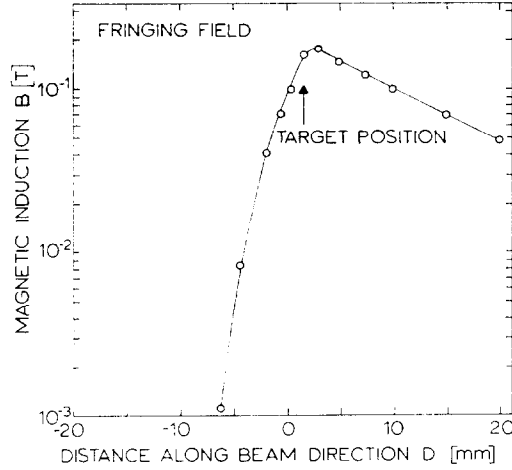


Fig. 3. Magnetic induction B along the beam axis. The zero distance corresponds to the end of the iron snout. The target was positioned at $d = 1.5$ mm, the Si detector at $d = -46$ mm.

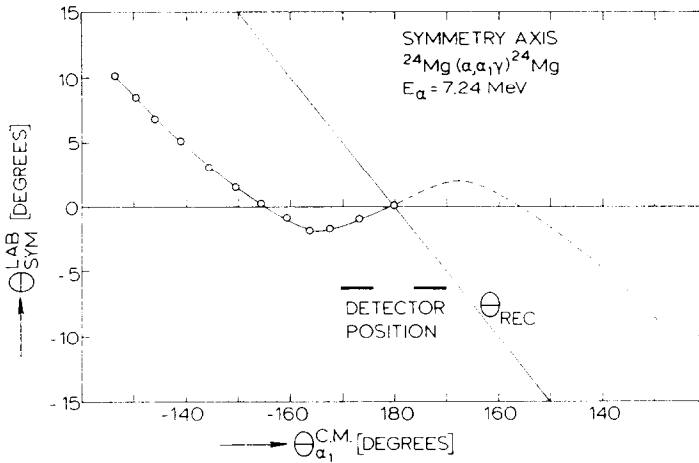


Fig. 4. The measured angular correlation symmetry axis for ^{24}Mg as a function of the outgoing α -particle detection angle (in the c.m. system). The adiabatic recoil direction, θ_{rec} , is shown, and the annular Si detector position in the present experiment is indicated.

bending rotation of $\Delta\theta_b = -0.3$ mrad is obtained¹⁵⁾, the negative sign indicating a rotation opposite to that of a nuclear state with a positive g -factor. This beam bending calculation, however, assumes that the symmetry axis (θ_{sym}) of the γ -ray angular correlation coincides with the recoil direction (θ_{rec}) of the excited nucleus. This is the case if the angular correlation theory is treated in the semi-classical¹⁶⁾, PWBA^{17,18)} or adiabatic¹⁹⁾ approximations, but for recoil energies exceeding the Coulomb barrier, in which case compound nucleus formation also becomes important, the assumption $\theta_{\text{sym}} = \theta_{\text{rec}}$ is not valid²⁰⁾.

Measurements of the beam bending yielded values of $\Delta\theta_b = 0.53 \pm 0.14$ and 0.79 ± 0.18 mrad for ^{24}Mg and ^{26}Mg , respectively (table 1). The deviation from the computed value can be understood quantitatively by measuring the axis of symmetry as a function of the α -particle detection angle. The results of a separate experiment for ^{24}Mg are shown in fig. 4. The experiment was performed by detecting γ -rays at 21 angles in four $12.7 \text{ cm} \times 12.7 \text{ cm}$ NaI(Tl) detectors in coincidence with α -particles detected between 126° and 167° in a position-sensitive detector. For the point at 173.6° an annular Si detector with an off-axial rectangular mask was used. The calculated rotation of the symmetry axis is composed of two parts, the bending of the incoming beam and the bending of the back-scattered α -particle trajectory. These yield rotations of $\Delta\theta_{\text{sym}}^{(1)} = 0.5$ mrad and $\Delta\theta_{\text{sym}}^{(2)} = 0.2$ mrad, respectively. Thus, the total expected beam bending rotation for ^{24}Mg of 0.7 mrad is in reasonable agreement with experiment.

2.5. DATA COLLECTION

The electronics set-up comprised the usual fast coincidence arrangement to obtain good time resolution. Coincidences between α -particles and γ -rays were determined with constant fraction timers and time-to-amplitude converters. The time resolution obtained was 3 ns (FWHM). The signals from the five γ -ray detectors, five time-to-amplitude converters and the particle detector were digitized by three ADC units interfaced with the CDC 1700 computer. The five γ -ray channels were mixed and fed into one ADC. The five time channels were treated similarly. A label bit pattern identified the active detector. To reduce pulse pile-up, dead time of the ADC and cross talk between the different γ -ray channels, a coincidence condition was applied by a linear gate immediately after each of the five main amplifiers used for γ -ray detection.

As a check on the electronics a pulser unit sent coincident pairs of pulses to the α -particle preamplifier and to each of the γ -ray preamplifiers in turn. These test signals were labelled separately to distinguish them from the γ -ray and α -particle spectra. In this way both the proper functioning of the labelling system and the absence of cross talk could be monitored. Peak stabilizers were used in the γ -ray channels to compensate for gain variations in the photomultipliers.

The direct α -particle spectrum was dominated by a plateau caused by the elastic scattering of α -particles from the Fe backing. A spectrum measured in coincidence with the 1.37 MeV γ -rays of ^{24}Mg is shown in fig. 5. This demonstrates the good particle discrimination obtained in these low- A measurements. A typical γ -ray spectrum coincident with the α_1 particle peak is shown in fig. 6.

The experiment was monitored by an on-line sorting procedure, using a disk for spectrum storage ²¹).

For the ^{24}Mg and ^{26}Mg experiments, 87 and 188 magnetic tapes, respectively, were required to store the event-by-event data. Each tape contained about 1.2×10^6 events. From the total number of events 5.6×10^6 and 3.3×10^6 useful coincidences were obtained for ^{24}Mg and ^{26}Mg , respectively.

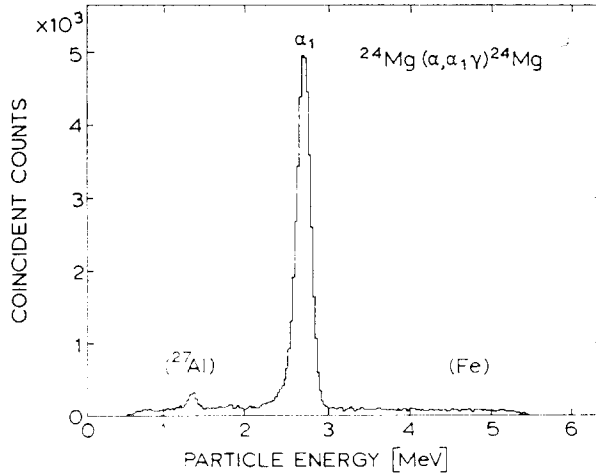


Fig. 5. A typical particle spectrum taken in coincidence with γ -rays from the 1.37 MeV level of ^{24}Mg . No random coincidences have been subtracted.

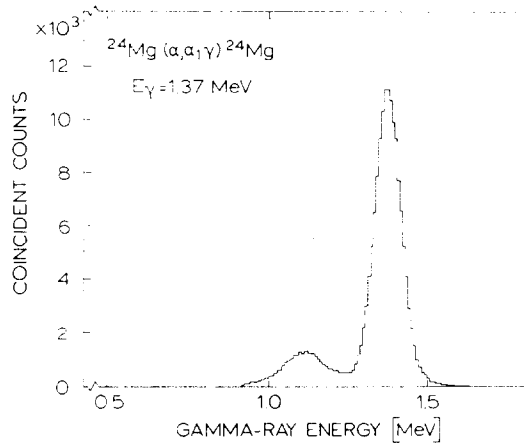


Fig. 6. A typical ^{24}Mg γ -ray spectrum taken in coincidence with α_1 particles detected at 180° . The spectrum is corrected for random coincidences. A threshold cuts out γ -rays with energies below 1.1 MeV.

3. Results and interpretation

3.1. STATISTICAL CONSIDERATIONS AND RESULTS

The mean precession angle $\Delta\theta$ can be expressed in terms of the relative change of γ -ray yield N measured at a certain angle θ by

$$\frac{\Delta N}{N} = \frac{1}{W} \frac{dW}{d\theta} \Delta\theta, \quad (1)$$

where

$$W(\theta) = \sum_{k=0,2,4} A_k Q_k Q'_k P_k(\cos \theta). \quad (2)$$

The quantities Q_k and Q'_k represent the geometrical attenuation coefficients due to the finite opening angles of the γ -ray detectors and the particle detector respectively; A_k and $P_k(\cos \theta)$ are the angular correlation coefficients and Legendre polynomials, respectively. The Q_k coefficients were taken from ref. ²²), and the measured correlation coefficients agreed with the theoretically expected values. The attenuation due to the finite size of the α -particle detector may be neglected since it merely causes a spread of 2° in the symmetry axis of the angular correlation (see fig. 4), i.e. $Q'_k = 1$.

The precession angle was determined from the ratio of coincident counts accumulated in the γ -ray detectors at $\pm(\frac{1}{2}\pi \pm \theta_1)$ rad with magnetic field up and down. The effect ε for one pair of detectors is defined by

$$\varepsilon = \left(\frac{N(\frac{1}{2}\pi + \theta_1)}{N(\frac{1}{2}\pi - \theta_1)} \right)_\uparrow \left(\frac{N(\frac{1}{2}\pi - \theta_1)}{N(\frac{1}{2}\pi + \theta_1)} \right)_\downarrow - 1 \approx \frac{4\Delta N}{N}. \quad (3)$$

The angle θ_1 can be chosen such that for a fixed measuring time and given values of Q_k , the relative error in ε is a minimum. For the present experiments, in which the 2^+ states are populated only in the $m = 0$ substate and then decay by a pure $2^+(E2) 0^+$ transition, the best value is $\theta_1 = 18^\circ$.

Large numbers of counts were required in order to obtain a sufficiently small statistical error in the net effect, corrected for beam bending. It was thus essential to demonstrate the absence of systematic trends in the data.

For four γ -ray detectors at fixed angles $\pm(\frac{1}{2}\pi \pm \theta_1)$, the cross ratios ε_c , given by

$$\varepsilon_c = \left(\frac{N(\frac{1}{2}\pi \pm \theta_1)}{N(-\frac{1}{2}\pi \pm \theta_1)} \right)_\uparrow \left(\frac{N(-\frac{1}{2}\pi \pm \theta_1)}{N(\frac{1}{2}\pi \pm \theta_1)} \right)_\downarrow - 1, \quad (4)$$

could be used to check the reliability of the measurements. These cross ratios were always zero within the statistical error.

As a further statistical check the effects ε and ε_c were analysed for each magnetic tape separately and the results plotted as a frequency distribution both for the

TABLE I
Summary of measured effects for ²⁴Mg and ²⁶Mg

Nucleus	Detector pair	Precession		Beam bending		$\Delta\theta = \Delta\theta_p - \Delta\theta_b$ (mrad)
		ε (%)	$\Delta\theta_p$ (mrad)	ε_b (%)	$\Delta\theta_b$ (mrad)	
²⁴ Mg	1,2	3.6 ± 0.3	2.0 ± 0.2	0.8 ± 0.4	0.4 ± 0.2	1.4 ± 0.2
	3,4	3.2 ± 0.3	1.8 ± 0.2	1.1 ± 0.4	0.6 ± 0.2	
²⁶ Mg	1,2	4.2 ± 0.5	2.4 ± 0.3	1.0 ± 0.5	0.6 ± 0.3	1.7 ± 0.3
	3,4	4.8 ± 0.5	2.7 ± 0.3	1.8 ± 0.5	1.0 ± 0.3	

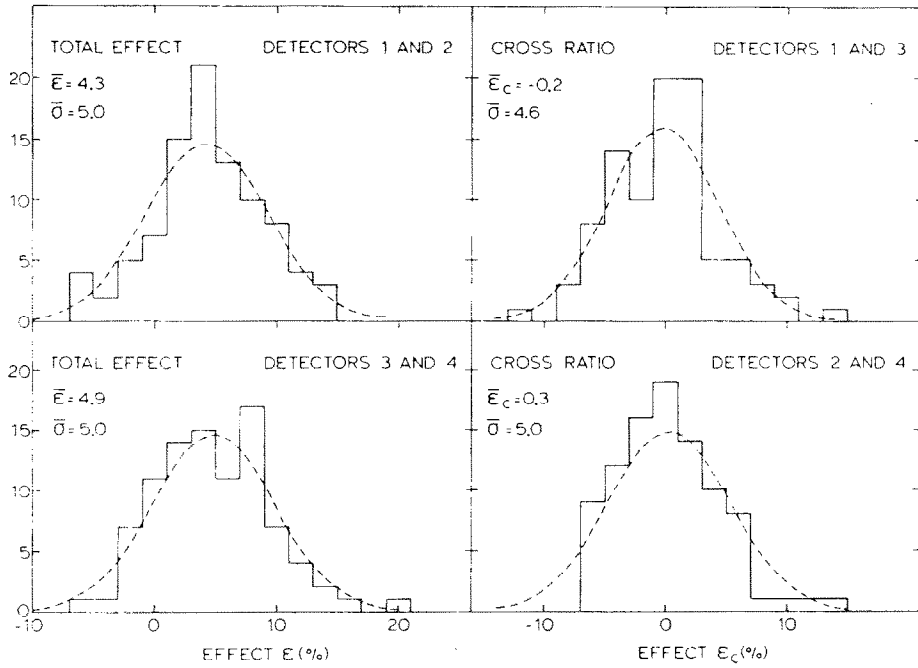


Fig. 7. Frequency distributions of the precession effects ϵ and cross ratios ϵ_c per tape for the ^{26}Mg experiment as calculated for the indicated detector pairs. The expected Gaussian distributions with expectation values $\bar{\epsilon}$ and standard deviations $\bar{\sigma}$ ($\bar{\sigma}$ is the average of the error per tape) are also shown.

precession and the beam bending measurements. For purely statistical errors such a frequency distribution is Gaussian with a standard deviation as large as that obtained for the effect for each tape. A typical example for the ^{26}Mg precession effects and cross ratios is shown in fig. 7. No significant deviations from Gaussian distributions were observed.

A summary of the measured precession and beam bending effects is given in table 1. The final statistical error in $\Delta\theta$ is in both cases 14 %.

3.2. THE TRANSIENT FIELD

In order to extract the g -factor from the observed precession, it is necessary to understand the dependence on the transient field. For this reason we discuss the Lindhard and Winther theory of the transient field ¹¹⁾ in some detail.

For a density of polarized electrons, which is spherically symmetric around the nucleus of the moving ion in a ferromagnet, which has a maximum there and which vanishes at infinity, the magnetic induction at the ion nucleus can be written ¹¹⁾

$$B(v) = \frac{2}{3}Q\zeta N\mu_e, \quad (5)$$

where Q is the total field enhancement factor and ζ , N and μ_e are the average number of polarized electrons per atom of the ferromagnetic material, the number of atoms

per m³ and the magnetic moment of the electron, respectively. The total enhancement factor is given by

$$Q = \bar{\chi}RP, \quad (6)$$

with, for an unscreened Coulomb potential, an enhancement factor of

$$\bar{\chi} = \frac{2\pi Z_1 v_0}{v_p} f(v), \quad (7)$$

where Z_1 , v_0 and v_p are the charge of the recoiling nucleus, the electron velocity in the first Bohr orbit ($c/137$) and the velocity of the polarized electrons, respectively, and the velocity factor $f(v)$ is defined as v_p/v for $v > v_p$ and unity otherwise. The relativistic correction R [see ref. ¹¹] is less than 1 % in the present case. The relative probability P for the ion to meet polarized electrons is normally taken to be unity but drops to zero for very low ion velocities, when the ion is no longer able to penetrate the electron shells of the ferromagnetic atom. For the present purposes P is chosen to be unity for $E_{\text{ion}} > 1$ keV and zero for $E_{\text{ion}} < 1$ keV. The actual choice of the cut-off energy, however, has little effect on the calculations since the initial ion energy is large in comparison.

The average rate of precession during slowing down is given by

$$d\phi = \frac{g\mu_n B(v)}{\hbar} dt, \quad (8)$$

where μ_n is the nuclear magneton and g the nuclear g -factor.

The total average precession $\phi(v)$ experienced by an ion with initial velocity v (after transforming the time variable to a velocity variable) is

$$\phi(v) = \frac{16}{9} \left(\frac{e^2}{\hbar c 4\pi\epsilon_0} \right)^2 \left(\frac{mZ_1 Z(A_1 + A_2)^3}{MZ_2 A_1 A_2} \right)^{\frac{1}{2}} g\zeta R \frac{v_0}{v_p} I(v), \quad (9)$$

where

$$I(v) = \int_{\epsilon_i}^0 P(\epsilon) f(\epsilon) \left(\frac{d\epsilon}{d\rho} \right)^{-1} d(\epsilon^{\pm}),$$

$$Z = (Z_1^{\frac{2}{3}} + Z_2^{\frac{2}{3}})^{\frac{3}{2}}.$$

The quantities m and M represent the electron mass and nucleon mass, and ϵ and ρ the recoil energy and recoil distance in a dimensionless representation ²³); $d\epsilon/d\rho$ denotes the stopping power. The initial recoil energy is ϵ_i and the suffixes on Z and A take the values of 1 and 2 for the recoiling and ferromagnetic nuclei, respectively.

One uncertainty entering into the theory is the value to be taken for the velocity of polarized electrons v_p . This was estimated by Lindhard and Winther to be somewhat less than v_0 . We have attempted a more exact estimate. From the binding energy of electrons in the 3d band of Fe, determined from X-ray emission ²⁴⁻²⁶) and also photoemission experiments ²⁷⁻²⁹), an average velocity $v_p = 0.78 v_0$ has

been calculated. For a proper estimate of v_p , however, it is important to know the probability distribution of the polarized electrons within the 3d band (i.e. the excess of spin-up over spin-down electrons). Calculations performed³⁰⁾ for the spin-up and spin-down electrons separately, yield reasonable agreement with experiment for the probability distribution of the total electron band, i.e. the sum of the spin-up and spin-down bands, and hence similar calculations should well describe the distribution for the excess. This yields an average value of $v_p = 0.81 v_0$, with the assumption of an unscreened Coulomb potential for the Fe atom. For a given binding energy, a screened potential would lead to a higher electron velocity and hence the values given above are lower limits.

In fig. 8 the transient field precession angle divided by the nuclear g -factor is plotted versus Z_1 . The theoretical curve is shown for $v_p = 0.78 v_0$. Although this curve follows the general experimental trend rather well, there remains an average discrepancy of about 40 %.

Another assumption made in the theory concerns the potential of the moving ion. In the derivation of eq. (7) Lindhard and Winther used an unscreened Coulomb potential. It would be more realistic to adopt a Thomas-Fermi-like screening of the potential by the electrons moving with the ion, as used in stopping theory^{31, 32)}. To estimate the effect of screening on the transient field precession, calculations were performed with the Hulthén potential¹¹⁾. This allows analytic solutions of the Schrödinger equation for the s -states that determine the enhancement factor. Averaging the enhancement factor $\bar{\chi}_H$, given by eq. (A.8) of ref.¹¹⁾, over the directions of the polarized electron velocity one obtains for $v > v_p$

$$\bar{\chi}_H = \chi \left[1 + 2 \sum_{n=1}^{\infty} (-1)^n e^{-4\pi n \lambda} \frac{\sinh 4\pi n \lambda_p}{4\pi n \lambda_p} \right], \quad (10)$$

where

$$\lambda = \frac{0.8853}{Z^{\frac{1}{2}}} \frac{v}{v_0},$$

$$\lambda_p = \frac{0.8853}{Z^{\frac{1}{2}}} \frac{v_p}{v_0}.$$

For $v < v_p$ the same formula applies with λ and λ_p interchanged. The phase factor $\cos(2\pi\beta)$ in eq. (A.8) of ref.¹¹⁾, which is very sensitive to the screening length used in the potential, has been averaged over all possible values.

Inclusion of screening decreases the precession angle by 20–40 % depending on the mean life and the initial velocity of the recoiling ion. The enhancement factors $\bar{\chi}$ at $v_p = 0.78 v_0$ with and without screening are plotted in fig. 9 for ^{24}Mg slowing down in Fe as a function of time. In this case the precession angle averaged over the lifetime decreases by 32 % if screening is included. The disagreement with experiment is greater with the inclusion of screening for $v_p = 0.78 v_0$ (see fig. 8). It is not obvious that the theory can be improved by a more refined calculation of the corrections in-

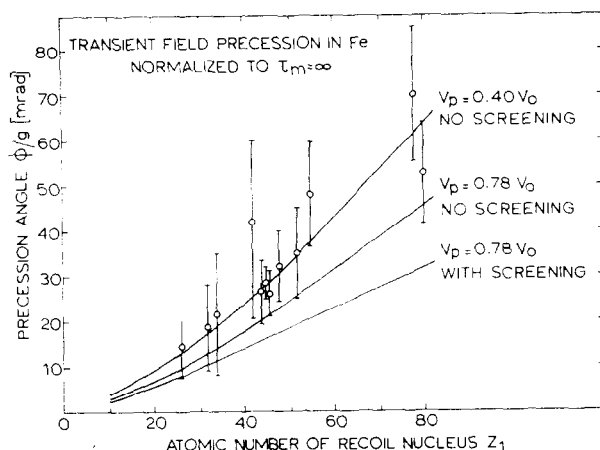


Fig. 8. The precession angle ϕ divided by the nuclear g -factor for implantation in iron, normalized to recoils from inelastically back-scattered 33 MeV ^{16}O and infinite lifetime. The curves are calculated from eq. (9) for $v_p = 0.78 v_0$, with and without screening. The curve fitted to the experimental data ($v_p = 0.40 v_0$) is also shown. The experimental points are from ref. ³⁵) for Fe, Ge, Se, Mo, Cd and Te; ref. ³⁷) for Ru and Pd; ref. ¹²) for Rh; ref. ³⁶) for Ba; ref. ³⁸) for Pt, but corrected for better known lifetimes ³⁹); ref. ⁴⁰) for Hg.

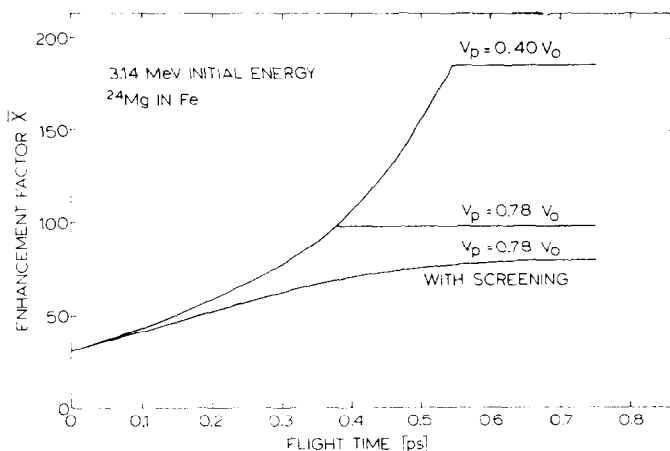


Fig. 9. The enhancement of the electron density \bar{X} for ^{24}Mg in Fe as a function of flight time for an initial recoil energy of 3.14 MeV; stopping time 0.75 ps. The curves for $v_p = 0.40 v_0$ and $v_p = 0.78 v_0$ are calculated with eq. (7) and the curve $v_p = 0.78 v_0$ with screening included, is calculated with eq. (10).

involved, although an estimate of a possible variation in the polarized electron cross section with the ion velocity might be worth attempting. As the uncertainty in v_p and the inclusion of screening have a similar effect on ϕ/g in eq. (9), it was decided to approximate reality by fitting v_p to the experimental results in the higher- A region and neglecting screening. This fit is also included in fig. 8. The value of v_p obtained

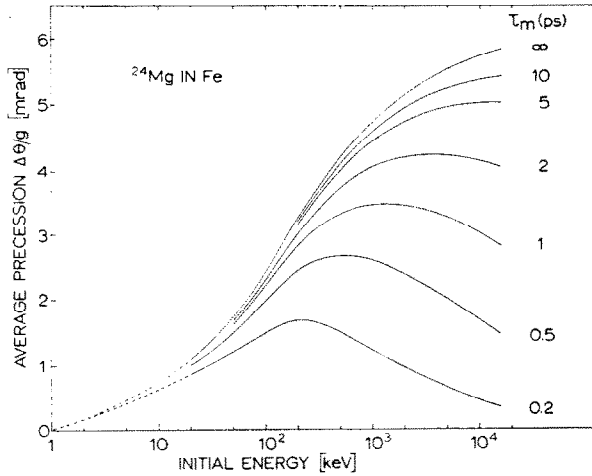


Fig. 10. The average precession angle $\Delta\theta$ divided by the nuclear g -factor for zero static field for $Z_t = 12$ as a function of the initial recoil energy with the excited-state lifetime as a parameter. The curves are calculated with eq. (11). A cut-off energy of 1 keV for the total enhancement factor Q is applied (see subsect. 3.1).

in this way $(0.40 \pm 0.08) v_0$ is now no longer a parameter with a strictly physical meaning. In ref. ¹³⁾ the precession angle has been measured as a function of the initial recoil energy for ^{56}Fe recoiling into a Fe backing. The theoretical expression was fitted to the experimental points with v_p and the g -factor as parameters. This yielded $v_p = (0.38 \pm 0.16) v_0$ in good agreement with the value obtained above from the Z -dependence.

Eq. (9) applies only to infinitely long-lived nuclear states. If the lifetime τ_m of the nucleus becomes comparable to the stopping time ($t_s \approx 1$ ps), an increasing proportion of the nuclei will decay in flight and hence the average precession will be reduced. The nuclei stopped completely before decaying, however, will precess further in the static magnetic hyperfine field of the lattice with Larmor frequency ω_s .

For small precession angles one obtains

$$W(\theta - \Delta\theta) = \frac{1}{\tau_m} \int_0^{t_s} W(\theta - \phi(t)) e^{-t/\tau_m} dt + e^{-t_s/\tau_m} W(\theta - \phi(t_s) - \omega_s \tau_m). \quad (11)$$

The average rotation $\Delta\theta/g$ as a function of the initial recoil energy, with the nuclear mean life as a parameter, is shown in fig. 10 for zero static field. For mean lives less than 2 ps, the precession has a maximum for a particular initial recoil velocity. The decrease at high velocities is due to a large fraction of nuclei decaying in flight before the full transient field is experienced. In the present experiment the initial recoil velocity for ^{24}Mg ($\tau_m = 1.75$ ps) resulted in the maximum precession, whereas for ^{26}Mg the initial recoil velocity necessary for a sufficient yield of the reaction gave rise to a precession 16 % below the maximum value.

3.3. INTERPRETATION

To deduce the g -factors from the experimental data (table 1) a computer program was written to calculate $W(\theta-\Delta\theta)$, see eq. (11). This program also takes into account the finite target thickness, the effect of which is to reduce the precession angle. The error calculus has been performed with this program by allowing a variation of the various quantities in the eqs. (9) and (11). The resulting relative errors in the g -factor produced by each of these quantities are given in table 2. The contribution of every quantity to the final quoted error will now be discussed in some detail.

TABLE 2
Sources of errors and their contributions to the error in g

Quantity	^{24}Mg		^{26}Mg	
	relative error (%)	contribution to g (%)	relative error (%)	contribution to g (%)
$\Delta\theta$	14	14	14	14
B_s	100	5	100	< 1
τ_m	5	1.2	10	9
v_p	22	11	22	8
$d\epsilon/d\rho$	15	13	15	2
d	30	3.3	30	11
ζ	5	5	5	5
total error 23 %			total error 22 %	

(i) *Static field B_s .* The static magnetic hyperfine field of Mg in Fe is not known. An estimate may be made by taking the systematic trends in series of elements with similar electron configurations, e.g. Ag and the following elements, and scaling these down to the known fields of the nearby elements Al and F in Fe [refs. ^{33,34}]. This yields a small field $B_s = -3 \pm 3$ T which gives rise to a 5 % correction for ^{24}Mg . For ^{26}Mg the static field contribution to $\Delta\theta$, $e^{-t_s/\tau_m}\omega_s\tau_m$, is ten times smaller and therefore negligible.

(ii) *Mean lives.* The adopted values for the mean lives of the ^{24}Mg and ^{26}Mg first excited states are 1.75 ± 0.08 and 0.48 ± 0.05 ps, respectively ²⁾. The sensitivity of the g -factor to variations of τ_m is to a good approximation proportional to $1/\tau_m$, and this leads to error contributions of 1.2 % and 9 % for ^{24}Mg and ^{26}Mg , respectively.

(iii) *Polarized electron velocity.* The fitted value for the polarized electron velocity, $v_p = (0.40 \pm 0.08) v_0$, is used in the calculations. Fig. 9 illustrates that the dependence of g on v_p increases with increasing lifetime τ_m . Thus the error contribution is somewhat larger for ^{24}Mg than for ^{26}Mg .

(iv) *Stopping power.* The stopping power theory of Lindhard, Scharff and Schiøtt [ref. ²³]] was used to describe the slowing-down of Mg ions in Fe, with the nuclear

stopping approximations of Curry ⁴¹). An uncertainty of 15 % in both the electronic and nuclear stopping powers was assumed. To understand the difference in error propagation for ²⁴Mg and ²⁶Mg, two effects on $\Delta\theta$ have to be considered separately. If the stopping power is reduced, the stopping time will increase, thus leading to an increased precession. However, the nuclei that decay in flight will contribute with a reduced precession, because they decay at higher velocity, corresponding to a lower transient field. The relative contributions of these two effects are determined by the mean life of the nuclear state. For ²⁶Mg the two contributions almost cancel, whereas for ²⁴Mg the first effect is predominant.

(v) *Target thickness.* The target thickness d specified in subsect. 2.1 resulted in a reduction of the average precession angle of 7 % for ²⁴Mg and 36 % for ²⁶Mg. The uncertainty in the target thickness was estimated to be 30 %. For ²⁶Mg this yields a large uncertainty (11 %) in the value of g because of the short lifetime.

(vi) *Number of polarized electrons per atom ζ .* The quantity ζ was measured as $\zeta = 2.02 \pm 0.08$ (subsect. 2.2). The error propagates linearly in g since the static field contributions are small.

The errors are treated independently and yield relative errors in the values of the g -factors for ²⁴Mg and ²⁶Mg of 23 and 22 %, respectively. This leads to final results for ²⁴Mg(2^+) and ²⁶Mg(2^+) of $g = +0.42 \pm 0.09$ and $g = +1.3 \pm 0.3$, respectively.

4. Conclusions

The transient magnetic field in Fe has been used successfully to measure magnetic dipole moments of very short-lived nuclear states in the sd shell, thus extending the applicability of such measurements, which have previously only been performed for $A \geq 54$. Although the measurements are rather painstaking with measured precessions of a few mrad, the effect of the static hyperfine field requires merely a small correction of the results, in contrast to the IMPAC measurements at higher A , in which the static field often contributes a large proportion of the effect.

The main uncertainty in the interpretation of the results stems from the difficulty of the Lindhard and Winther ¹¹) theory in reproducing the magnitude of the transient field although the energy and atomic number dependence are well described. This

TABLE 3
Comparison of experimental and theoretical g -factors

Nucleus	Experiment	Shell model ^{a)} single shell	Shell model ^{a)} multi shell	Projected ^{b)} Hartree-Fock	SU(3) ^{c)}
²⁴ Mg(2_1^+)	$+0.42 \pm 0.09$ $\pm 0.44 \pm 0.04$ ^{d)}	$+0.58$	∓ 0.57	∓ 0.57	∓ 0.50
²⁶ Mg(2_1^+)	$+1.3 \pm 0.3$		$+0.91$	∓ 0.53	

^{a)} Ref. ⁴²). ^{b)} Ref. ⁴³). ^{c)} Ref. ⁴⁵). ^{d)} Ref. ³).

difficulty has been overcome by fitting the theory to all previous results in the higher- A region and extrapolating to Mg. The effectiveness of this procedure is confirmed by the good agreement of the extracted value of the ^{24}Mg g -factor with the result 0.44 ± 0.04 of a more recent measurement³⁾ with the time-differential recoil-into-vacuum technique.

The experimental values of the g -factors of the first excited ^{24}Mg and ^{26}Mg states are compared with those of some theoretical calculations in table 3. In shell-model calculations⁴²⁾ an MSDI effective two-body interaction was used with the configuration space limited to $1d_{5/2}$ and to $1d_{3/2}$, $2s_{1/2}$ shells. Hartree-Fock calculations⁴³⁾ use a configuration space of the first five major oscillator shells and an effective two-body interaction. For ^{24}Mg these three calculations yield a value for the g -factor which is slightly too large. For the shell-model calculations⁴⁴⁾ better agreement is obtained if $1d_{3/2}$ contributions are included ($g = 0.52$). Better agreement with experiment is achieved by an SU(3) calculation⁴⁵⁾ in which complete sd configurations are used.

For ^{26}Mg the Hartree-Fock calculation⁴³⁾ is off by about 2.5 standard deviations whereas the shell model value⁴⁶⁾ is only slightly low.

The authors gratefully acknowledge fruitful discussions with Dr. H. A. Doubt and his critical reading of the manuscript. They also thank N. A. van Zwol and D. Balke for the construction of the experimental set-up. This work was performed as a part of the research program of FOM with financial support from the "Nederlandse Organisatie voor Zuiver-Wetenschappelijk Onderzoek" (ZWO).

References

- 1) P. W. M. Glaudemans, P. M. Endt and A. E. L. Dieperink, *Ann. of Phys.* **63** (1971) 134; B. H. Wildenthal and J. B. McGrory, *Phys. Rev.* **C7** (1973) 714
- 2) P. M. Endt and C. van der Leun, *Nucl. Phys.* **A214** (1973) 1
- 3) R. E. Horstman, J. L. Eberhardt, H. A. Doubt and G. van Middelkoop, *Phys. Lett.* **48B** (1974) 31
- 4) A. Iordachescu, E. A. Ivanov and G. Pascovica, *Phys. Lett.* **48B** (1974) 28
- 5) D. Gordon, M. Ulrickson, R. Hensler, N. Benczer-Koller and J. R. MacDonald, *Bull. Am. Phys. Soc.* **19** (1974) 17
- 6) F. Brandolini, C. Rossi Alvarez, G. B. Vingiani and M. De Poli, *Phys. Lett.* **49B** (1974) 261
- 7) L. Grodzins, *Hyperfine structure and nuclear radiations*, ed. E. Matthias and D. A. Shirley (North-Holland, Amsterdam, 1968) p. 607
- 8) R. R. Borchers, J. Bronson, D. E. Murnick and L. Grodzins, *Phys. Rev. Lett.* **17** (1966) 1099
- 9) B. Herskind, R. R. Borchers, J. Bronson, D. E. Murnick, L. Grodzins and R. Kalish, *Hyperfine structure and nuclear radiations*, ed. E. Matthias and D. A. Shirley (North-Holland, Amsterdam, 1968) p. 735
- 10) R. R. Borchers, B. Herskind, J. Bronson, L. Grodzins, R. Kalish and D. E. Murnick, *Phys. Lett.* **20** (1968) 424
- 11) J. Lindhard and A. Winther, *Nucl. Phys.* **A166** (1971) 413
- 12) R. Heusinger, W. Kreische, W. Lampert, K. Reuter, K. H. Roth and K. Thomas, internal report Physikalisches Institut der Universität Erlangen-Nürnberg
- 13) G. K. Hubler, H. W. Kugel and D. E. Murnick, *Phys. Rev. Lett.* **29** (1972) 662
- 14) G. M. Heestand, P. Hvelplund, B. Skaali and B. Herskind, *Phys. Rev.* **B2** (1970) 3698

- 15) G. Goldring, R. Kalish and H. Spehl, Nucl. Phys. **80** (1966) 33
- 16) S. T. Butler, N. Austern and C. Pearson, Phys. Rev. **112** (1958) 1227
- 17) G. R. Satchler, Proc. Phys. Soc. **68** (1955) 1037
- 18) A. B. Clegg and G. R. Satchler, Nucl. Phys. **27** (1961) 431
- 19) J. S. Blair and L. Wilets, Phys. Rev. **121** (1961) 1493
- 20) W. W. Eidson, J. G. Cramer, D. E. Blatchley and R. D. Bent, Nucl. Phys. **55** (1964) 613
- 21) P. B. J. van Elswijk, R. Engmann, A. M. Hoogenboom and P. de Wit, Nucl. Instr. **96** (1971) 35
- 22) A. R. Rutledge, A.E.C.L.-report CRP-851, Chalk River (1964)
- 23) J. Lindhard, M. Scharff and H. H. Schiøtt, Mat. Fys. Medd. Dan. Vid. Selsk. **33** no. 14 (1963)
- 24) E. M. Gyorgy and G. G. Harvey, Phys. Rev. **93** (1954) 365
- 25) H. W. B. Skinner, T. G. Bullen and J. E. Johnston, Phil. Mag. **45** (1954) 1070
- 26) D. H. Tomboulion and D. E. Bedo, Phys. Rev. **121** (1961) 146
- 27) A. J. Blodgett and W. E. Spicer, Phys. Rev. **158** (1967) 514
- 28) C. S. Fadley and D. A. Shirley, Phys. Rev. Lett. **21** (1968) 980
- 29) D. E. Eastman, J. Appl. Phys. **40** (1969) 1387
- 30) S. Wakoh and J. Yamashita, J. Phys. Soc. Jap. **21** (1966) 1712
- 31) J. Lindhard, V. Nielsen and M. Scharff, Mat. Fys. Medd. Dan. Vid. Selsk. **36** no. 10 (1968)
- 32) P. Gombás, Handbuch der Physik **36**, p. 120
- 33) D. A. Shirley, Hyperfine structure and nuclear radiations, ed. E. Matthias and D. A. Shirley (North-Holland, Amsterdam, 1968) p. 979
- 34) I. A. Campbell, Proc. Roy. Soc. **A311** (1969) 131
- 35) G. M. Heestand, R. R. Borchers, B. Herskind, L. Grodzins, R. Kalish and D. E. Murnick, Nucl. Phys. **A133** (1969) 310
- 36) H. W. Kugel, T. Polga, R. Kalish and R. R. Borchers, Phys. Lett. **32B** (1970) 463
- 37) G. K. Hubler, Ph.D. thesis, Rutgers University (1972);
G. K. Hubler, H. W. Kugel and D. E. Murnick, Phys. Rev. **C9** (1974) 1954
- 38) H. W. Kugel, R. R. Borchers and R. Kalish, Nucl. Phys. **A137** (1969) 500
- 39) H. A. Doubt, J. B. Fechner, K. Hagemeyer and K.-H. Speidel, Z. Phys. **254** (1972) 339
- 40) A. F. Dilmanian and R. Kalish, Phys. Rev. **B8** (1973) 3093
- 41) W. M. Curry, Nucl. Instr. **73** (1969) 173
- 42) J. F. A. van Hienen and P. W. M. Glaudemans, Phys. Lett. **42B** (1972) 301
- 43) M. R. Gunye, Phys. Lett. **37B** (1971) 125
- 44) J. Koops, University of Utrecht, private communication
- 45) D. Strottman, Phys. Lett. **39B** (1972) 457
- 46) J. F. A. van Hienen, P. W. M. Glaudemans and J. van Lidth de Jeude, Nucl. Phys. **A225** (1974) 119
- 47) Proc. Int. Conf. on hyperfine interactions studied in nuclear reactions and decay, Uppsala, 1974, ed. E. Karlsson and R. Wäppling